Am J Nucl Med Mol Imaging 2013;3(4):300-311
www.ajnmmi.us /ISSN:2160-8407/ajnmmi1304001

Original Article

Molecular MRI differentiation of VEGF receptor-2 levels in C6 and RG2 glioma models

Ting He[1,2], Nataliya Smith[1], Debra Saunders[1], Benjamin P Pittman[1], Megan Lerner[3], Stanley Lightfoot[4], Robert Silasi-Mansat[5], Florea Lupu[5], Rheal A Towner[1,2,4]

[1]Advanced Magnetic Resonance Center, [5]Cardiovascular Biology, Oklahoma Medical Research Foundation, Oklahoma City, OK 73104 USA; [2]Oklahoma Center for Neuroscience, [3]Department of Surgery, [4]Department of Pathology, University of Oklahoma Health Sciences Center, Oklahoma City, OK 73104 USA

Received April 15, 2013; Accepted June 21, 2013; Epub July 10, 2013; Published July 15, 2013

Abstract: Vascular endothelial growth factor receptor 2 (VEGFR2) is an important angiogenic marker over-expressed in gliomas. With the use of molecular magnetic resonance imaging (mMRI) differing levels of VEGFR2 can be characterized *in vivo* with in rodent gliomas varying in angiogenesis. VEGFR2 levels were assessed by intravenous administration of an anti-VEGFR2 probe (anti-VEGFR2-albumin-Gd (gadolinium)-DTPA (diethylene triamine penta acetic acid)-biotin) into C6 or RG2 glioma-bearing rats, and visualized with mMRI. A non-specific IgG was coupled to the albumin-Gd-DTPA-biotin construct as a contrast agent molecular weight control. VEGFR2 levels are heterogeneous in different regions of C6 gliomas, whereas VEGFR2 was more homogenous or evenly distributed in RG2 gliomas. RG2 gliomas have less VEGFR2 within tumor periphery and peri-necrotic ($p<0.05$) regions, but more VEGFR2 within tumor interior regions ($p<0.01$), compared to C6 gliomas. mMRI results were confirmed with fluorescence staining and mean fluorescence intensity (MFI) quantification of the anti-VEGFR2 probe in excised glioma and brain tissues, as well as detection of VEGFR2 in C6 and RG2 gliomas and corresponding contalateral brain tissues. *Ex vivo* VEGFR2 levels were found to be significantly higher in C6 gliomas compared to RG2 tumors ($p<0.001$), which corresponded with *in vivo* detection using the VEGFR2 probe. Immunohistochemistry staining for HIF-1α (hypoxia inducible factor 1α), which is associated with angiogenesis, indicated higher levels in RG2 ($p<0.01$) compared to C6 gliomas. The data suggests that C6 gliomas have angiogenesis which is associated more with large blood vessels in tumor periphery and peri-necrotic regions, and less microvascular angiogenesis within the tumor interior, compared to RG2 gliomas.

Keywords: Molecular magnetic resonance imaging (mMRI), vascular endothelial growth factor receptor 2 (VEGFR2), C6 and RG2 rat gliomas, *in vivo*, fluorescence imaging

Introduction

Gliomas are the most common primary brain tumors in the adult [1]. It has been demonstrated that angiogenesis is greatly upregulated in high-grade gliomas compared to low-grade gliomas [2]. Angiogenesis is an essential process that provides excess nutrients to developing tumors even at a very early stage [3]. Assessing angiogenesis is one of the most important criteria for grading tumors in patients [4].

Angiogenesis is driven by a multiple, complicated network which involves the interaction of a number of pro-angiogenic factors and endogenous angiogenic inhibitors. Vascular endothelial growth factor (VEGF) is the most important stimulant factor in regulating angiogenesis. Stimulation of VEGF by interacting with one of its receptors, VEGF Receptor-2 (VEGFR-2), triggers endothelial cell proliferation, migration, survival, as well as an increase in vascular permeability through signaling pathways, including the phosphatidylinositol 3' kinase (PI3K)/Akt and the Ras/mitogen-activated protein kinase (MAPK) pathways [5]. VEGFR-2 is upregulated in tumor vasculature and mainly found on activated angiogenic endothelial cells [6, 7]. An accurate *in vivo* assessment of VEGFR-2 can provide an excellent approach to characterize active angiogenesis.

The rat C6 glioma model is the most commonly used model in the laboratory for characterizing

gliomas. The RG2 glioma model is a good model for human glioblastoma (GBM), a high grade glioma, due to its invasive growth pattern [8]. RG2 gliomas are more aggressive than C6 gliomas, as indicated by histology [9], and by tumor doubling times [10]. The microvasculature evolves differently in the two glioma models, as detected from the blood volume fraction (BVf) and the vessel size index (VSI) in the tumor center and the peripheral regions [10]. Efforts have been made to target specific markers for tumor angiogenesis like $\alpha_v\beta_3$-integrin, E-selectin, and aminopeptidase N using antibodies or peptides with molecular MRI, providing an important non-invasive imaging method for detecting angiogenesis [11-13]. Our previous work on molecular targeting of VEGFR-2 in C6 gliomas, indicated that there are heterogeneous levels of VEGFR-2 associated with the development of tumors and associated neovasculature [14]. In the current study we demonstrated that the levels of VEGFR-2 in C6 and RG2 gliomas are differentiated, as assessed bythe use of mMRI with a targeting anti-VEGFR-2 gadolinium-based contrast agent. The different VEGFR-2 levels detected by the anti-VEGFR-2 probe in these two glioma models indicates unique angiogenic profiles for each glioma. This method can provide an *in vivo* approach that can be used to assess angiogenesis. Comparative levels of the hypoxia inducible factor 1α, which is associated with angiogenesis, via immunohistochemistry was also assessed in C6 and RG2 gliomas.

Materials and methods

Synthesis of anti-VEGFR-2 MRI agent

The contrast agent, biotin-BSA (bovine serum albumin)-Gd-DTPA, was prepared as previously described by our group [17], based on the modification of the method developed by Dafni*et al*. [18]. The estimated molecular weight for the biotin-albumin-Gd-DTPA moiety is ~80 kDa. It is estimated that there are 1.3 biotin and 23 Gd-DTPA groups bound to each BSA molecule. Briefly, anti-VEGFR-2 mAb (Santa Cruz Biotech, Inc., CA, USA) was conjugated to the albumin moiety through a sulfo-NHS-EDC link according to the protocol of Hermanson [19]. Each animal was injected with 200 µl anti-VEGFR-2-BSA-Gd-DTPA-biotin (VEGFR-2 probe) intravenously (i.v.) via the tail vein with an amount estimated to be 200 µg anti-VEGFR-2 and 100 mg biotin-BSA-Gd-DTPA per injection (i.e. an excess amount of the contrast agent construct to antibody was added to ensure a 1:1 ratio of antibody to contrast agent for the complete anti-VEGFR2 probe, and then waiting at least 2 hours post-injection results in excess non-specific biotin-BSA-Gd-DTPA being eliminated). The estimated molecular weight of the VEGFR-2 probe is 232 kDa. As a control, normal rat-IgG (obtained from a healthy rat population; Alpha Diagnostic International, San Antonio, TX, USA) conjugated to biotin-BSA-Gd-DTPA (control-IgG contrast agent) was synthesized by the same protocol, and injected in a similar fashion, as described above.

In vitro characterization of anti-DMPO probe

Vials were prepared containing either water (no cells), rat primary astrocytes (ATCC, Manassas, VA, USA) alone, C6 or RG2 rat glioma cells alone, or either astrocytes, C6 or RG2 cells (ATCC) in the presence of the anti-VEGFR2 probe. Cells were grown in flasks in complete growth medium (DMEM Media with 10% fetal bovine serum (FBS), Invitrogen, Grand Island, NY, USA) to confluency. Two to three hours before treatment, the growth medium was replaced with serum-free medium. The anti-VEGFR2 probe was added (2 µg, based on antibody calculation), and cells were incubated for 45 min. Following incubation, cells were collected, washed with PBS, centrifuged (500 rpm), and the pellet was resuspended in PBS for MR imaging.

Intracerebral glioma cell implantation

All animal experiments were approved by the OMRF IACUC and follow the guidelines outlined by the National Research Council Guide for the care and use of laboratory animals. The intracerebral implantation of C6 or RG2 glioma cells was performed as previously published by our group [15]. Briefly, three-month-old male Fischer 344 rats (250-300 g, Harlan Laboratories, Indianapolis, IN, U.S.A.) were anesthetized with 2.0-2.5% isoflurane and 0.8 L/min oxygen, and immobilized on a stereotaxic unit (Stoelting Co., USA). Ten thousand (10^4) C6 or RG2 cells in 10 µL cell culture media and 1% ultra-low gelling temperature agarose (Sigma) were injected into the cortex at a 3 mm depth from the dura at a rate of 2 µL/min, in a location of 2 mm lateral and 2 mm anterior to the

bregma. Rats were fed with a choline-deficient (CD) diet to encourage the tumor cell growth for C6 gliomas after surgery [16].

Molecular MRI

MRI experiments were performed on a Bruker Biospec 7.0 Tesla/30 cm horizontal-bore magnet small animal imaging system (Bruker Biospin, Ettlingen, Germany). For the *in vitro* study, signal intensities were obtained using FLASH (Fast Low Angle SHot) [repetition time (TR) 125.3 ms, echo time (TE) 6.0 ms, 256×128 matrix, 4 steps per acquisition, 4.00×4.00 cm^2 field of view (FOV), 1 mm slice thickness]. T_1 maps were obtained using a RARE (Rapid Aquisition variable TR sequence (TR 200, 400, 800, 1200 and 1600 ms; TE 15 ms; 256×256 matrix; 2 steps per acquisition; 4.00×4.00 cm^2 FOV; slice thickness 1.0 mm). Pixel-by-pixel relaxation maps were reconstructed from a series of T_1-weighted images using a nonlinear two-parameter fitting procedure. For the in vivo study, animals were restrained by using 1-2% isoflurane in 0.8 L/min O_2, and placed in a radiofrequency (RF) resonator MR probe (72 mm quadrature volume coil) for signal transmission, and a rat head surface coil was used for signal reception. Animals were regularly monitored for tumor growth. T_2-weighted images were acquired for measuring tumor volumes using a rapid-acquisition relaxation enhanced sequence (RARE). Molecular MRI was performed when the tumor volumes were close to their maximum tumor volumes. A variable-TR RARE sequence (rapid acquisition with refocused echoes, with multiple TRs of 200, 400, 800, 1200 and 1600 ms, TE of 15 ms, FOV of 3.5×3.5 cm^2, matrix size of 256×256 and a spatial resolution of 0.137 mm) was used to obtain T_1-weighted images before and after administration of probe or control contrast agents. The changes in signal intensities were calculated from regions of interest (ROIs) obtained from T_1-weighted images. Four groups of ROIs were chosen as follows: tumor periphery (PT), peri-necrotic area (PN), tumor interior (TI) with a minimal signal intensity change and not associated with a necrotic area, and normal brain tissue (N) found on the contralateral side.

Fluorescence staining

The rat brains were extracted after the 2-hour mMRI protocol, the tumor side (tumor periphery) and contralateral side of the brain were cut and fixed in Z-fixative (Zinc Formalin: Formaldehyde 3.7%, Zinc Sulfate). The tissue was then washed with PBS and incubated with 15% sucrose before embedding in an Optimal Cutting Temperature (O.C.T.) compound and freezing in liquid nitrogen. The cryosections were then stained with Cy3-labeled streptavidin, which can bind to the biotin moiety of the albumin-Gd-DTPA-biotin contrast agent within the brain tissue. The nucleus was stained with DAPI (blue). Stained tissue slices were examined with a Nikon C1 confocal laser scanning microscope (Nikon Instruments, USA). Image collection parameters (neutral density filters, pinhole, and detector gains) were kept constant during image acquisition, to make reliable comparisons between specimens. The measurement of fluorescence intensity was done as previously described [20]. In brief, 5 images were collected for each experimental condition, and the mean fluorescence intensity (MFI) within 15-20 regions-of-interest (ROI) per image was integrated using the EZ-C1 software (Nikon).

Histology and immunohistochemistry (IHC)

A separate group of C6 and RG2 gliomas-bearing rats were euthanized when their tumors reached their maximum volumes. Brain tissues were extracted and fixed in 10% neutral buffered formalin, embedded in paraffin, and sectioned in 5 μm sections for routine staining. Sections were deparaffinized and rehydrated through three changes of xylene and graded alcohol, and stained with hematoxylin and eosin (H&E). The brain tissues sections were examined for VEGFR-2 using the anti-VEGFR-2 antibody (LS-C117508; rabbit polyclonal; anti-human/mouse/rat; Lifespan Biosciences, Inc., Seattle, WA, USA) or HIF-1α using the anti-HIF1 alpha antibody (EP1215Y; rabbit monoclonal; anti-rat and anti-human; 1/100 dilution; Abcam Inc., Cambridge, MA, USA), followed by Rat HRP-Polymer system (Biocare Medical, Concord, CA, USA) for detection and NovaRed (Vector Laboratories, Inc., Burlingame, CA, USA) chromogen for visualization. IHC scoring (0-12) was done using the following scoring scale: 0-2=negative, 3=weakly positive, 4-5=moderately positive, and 6-12=highly positive.

Western blot

VEGFR2 protein levels in either normal rat brain of C^- or RG2-glioma tissue from tumor-bearing

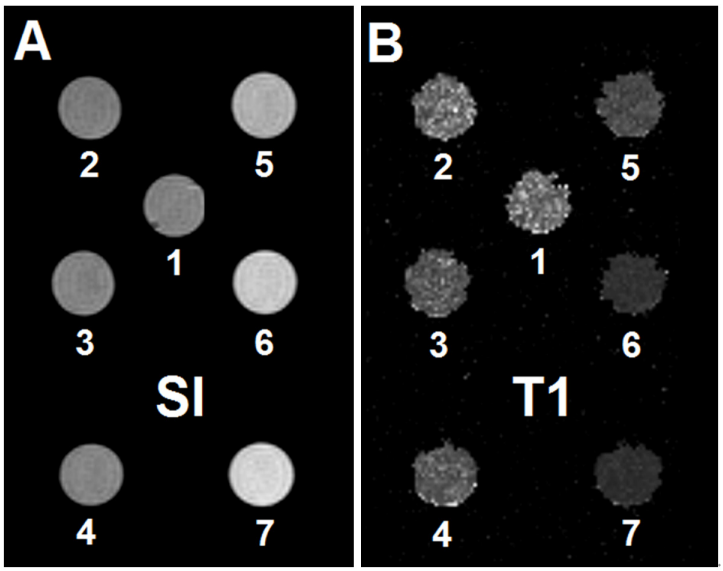

Figure 1. *In vitro* assessment of the anti-VEGFR2 probe in rat glioma cells. A: MRI signal intensities (SI) (T_1-weighted) and (B) T_1 maps (T1) of vials containing either (1) water, (2) primary rat astrocytes alone, (3) C6 rat glioma cells alone, (4) RG2 rat glioma cells alone, (5) astrocytes plus the anti-VEGFR2 probe, (6) C6 cells plus the anti-VEGFR2 probe, or (7) RG2 cells plus the anti-VEGFR2 probe.

animals was assessed by western blotting. Rat glioma or normal brain tissues were obtained as follows. Cardiac perfusion with PBS was performed while the rats were under anesthesia (Isoflurane), and then the heads were cut off using a guillotine. The skin and the muscles were removed from the head. Then the bones on the top of the head were carefully removed, from the cerebellum to the olfactory bulb through the bregma, and from one side of the head to the other side. The ear bones were carefully extracted from the brain; the optic chiasm and the olfactory bulb were excised in order to extract the brain. A transverse cut was then performed to get samples for Western blot assessment, which were immediately frozen in dry ice. Tissue was homogenized in ice-cold Tris-HCl buffer containing protease and phosphatase inhibitor cocktails (Roche Applied Science, Indianapolis, IN, USA). Protein concentration was measured with BCA Protein Assay (Thermo Scientific, Rockford, IL, USA). Protein electrophoresis was done in 4-15% gradient precast polyacrylamide gels (Biorad, Hercules, CA, USA), and protein was transferred to PVDF Immobillon-FL membrane (Millipore, Billerica, MA, USA). A mouse monoclonal anti-VEGFR2 for detection of VEGFR2 of mouse, rat or human origin by Western blotting (Santa Cruz Biotechnology, Inc., Santa Cruz, CA, USA) was incubated overnight at 1:500 dilutions in an Odyssey Blocking Buffer. Membranes were washed three times over 5 minutes with PBS and incubated with secondary antibodies for 1 hour at room temperature. Membranes were scanned in an Odyssey Infrared Imaging System (Li-Cor Biosciences, Lincoln, Nebraska, USA).

Statistical analysis

Statistical analyses were performed by using a Student's two-tailed, unpaired *t*-test for comparison of MR signal intensity increase percent ages between RG2 and C6 gliomas. Statistical analyses were performed by using a One Way Analysis of Variance with a post Tukey's multiple comparison test for comparison of Mean Fluorescence Intensity for the fluorescence imaging of the anti-VEGFR-2 probe and IHC of VEGFR-2 levels among all groups. Data were represented as mean±S.D. and *P*-values<0.05 (*), <0.01 (**), <0.0001 (***) were considered statistically significant.

Results

In vitro anti-VEGFR2 probe characterization in rat glioma cells

Figure 1 presents *in vitro* data regarding the effect of the anti-VEGFR2 probe on MRI signal intensity (SI) and T_1 relaxation in rat primary astrocytes, C6- or RG2-rat glioma cells. **Table 1** depicts the T_1 relaxation values (ms) in either astrocyes, C6 or RG2 rat glioma cells either alone or in the presence of the anti-VEGFR2 probe. Alls cells in the presence of the anti-VEGFR2 probe had decreased T_1 values, compared to cells alone or water. Both C6 and RG2 glioma cells had more of the anti-VEGFR2 present on their cells (due to decreased T_1) compared to the astrocytes.

In vivo assessment of VEGFR-2 levels in C6 and RG2 gliomas

Before administration of either the VEGFR-2 probe or the IgG isotype contrast agent, morphological T_2-weighted MR images were

Table 1. T1 relaxation values (ms) of vials containing (1) water, (2) primary astrocytes (Ast) alone, (3) C6 glioma cells (C6) alone, (4) RG2 glioma cells (RG2) alone, (5) Ast and the anti-VEGFR2 probe (Ast+VEGFR2 P), (6) C6 and VEGFR2 P (C6+VEGFR2 P), or (7) RG2+VEGFR2 P. Values are listed as mean±S.D. (n=3 per sample group)

T1 (ms)						
1	2	3	4	5	6	7
Water	Astrocytes (Ast)	C6 cells	RG2 cells	Ast+VEGFR2 P	C6+VEGFR2 P	RG2+VEGFR2 P
2099±25	2013±62	1653±45	1704±56	1463±18	1046±19	1003±17

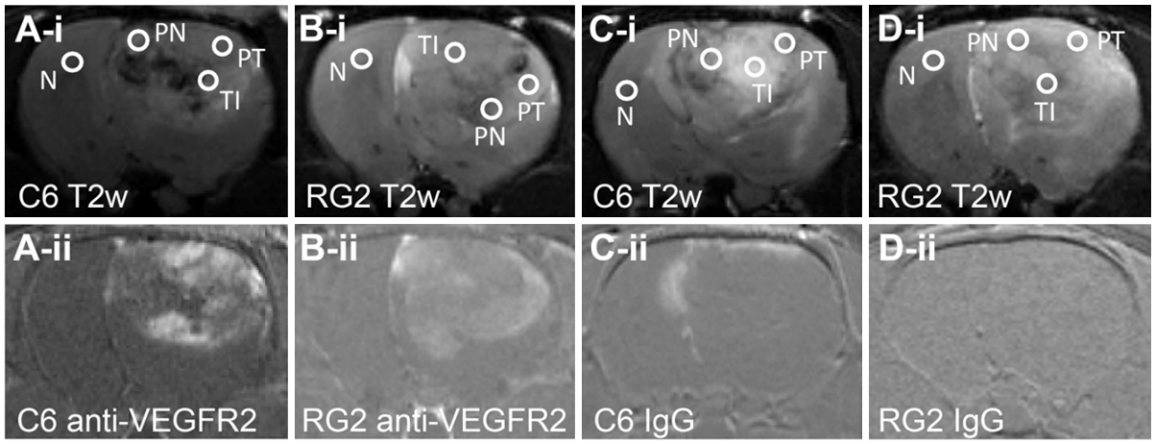

Figure 2. Differences in VEGFR2 probe distribution between C6 and RG2 glioma models. The four images in the top panel are T_2-weighted images of representative gliomas. A-i: AC6 tumorbefore injection of the anti-VEGFR2 probe (tumor volume=186 mm^3). B-i: ARG2 tumor before injection of the anti-VEGFR2 probe (tumor volume=143 mm^3). C-i: AC6 tumorbefore injection of the control-IgG contrast agent (tumor volume=189 mm^3). D-i: A RG2 tumor before injection of the control-IgG contrast agent (tumor volume=138 mm^3). Outlined areas (circles) for subsequent analysis (post-contrast) include 'normal' brain (N), tumor interior (TI), peri-tumor (PT) and peri-necrotic (PN) regions. The four images in the bottom panel (A-ii-D-ii) are difference images subtracted from T_1 weighted images obtained before and 2 hours post administration of either the probe (A-ii or B-ii) or isotype IgG contrast agent (C-ii or D-ii) in either C6 (A-ii and C-ii) or RG2 (B-ii and D-ii) gliomas.

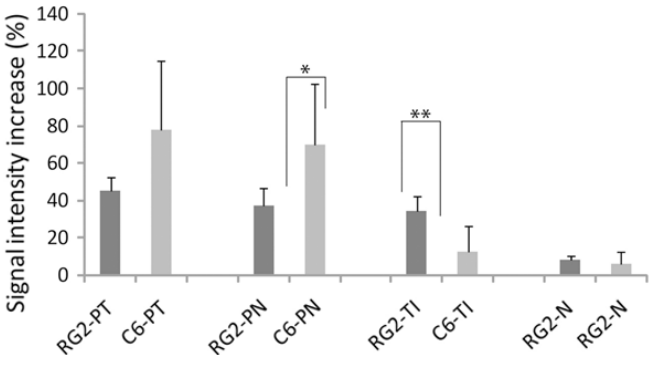

Figure 3. Signal intensity increase percentage (%) in T_1 weighted images induced by binding of VEGFR2 probe at 2 hours post administration of probe in different regions in C6 (9 regions-of-interest (ROIs) in 3 gliomas/animal) and RG2 (6 ROIs in 2 gliomas/animal) gliomas. The signal intensity increase (%) was calculated over the signal intensity before the administration of VEGFR2 probe. Data is represented as mean±S.D. *P<0.05, and **P<0.01, indicate the significant difference between RG2 and C6 in PN and TI region, by using two-tailed unpaired *t* test.

obtained to localize the tumors (e.g. **Figure 2A-i** and **2C-i** for C6 gliomas, or **Figure 2B-i** or **2D-i** for RG2 gliomas). A representative C6 glioma with a volume of 186 mm^3 and extensive necrotic areas at day 28 post tumor cell implantation is shown in **Figure 2A-i**. The average tumor volume for the C6 gliomas was 175±9 mm^3 (mean±S.D.), and the maximum tumor volumes were obtained 22±6 days following intracerebral implantation of C6 cells. A representative RG2 glioma with a tumor volume of 143 mm^3 at day 14 post cell implantation is shown in **Figure 2B-i**. The average tumor volume for the RG2 gliomas was 140±13 mm^3 (mean±S.D.), and the maximum tumor volumes were obtained 15±2 days following intracerebral implantation of RG2 cells. After administration of molecular targeting agents (either a VEGFR-2 probe or a non-specific control-IgG isotype contrast agent), T_1-weighted images were taken every 20 minutes continuously up to 120 minutes.

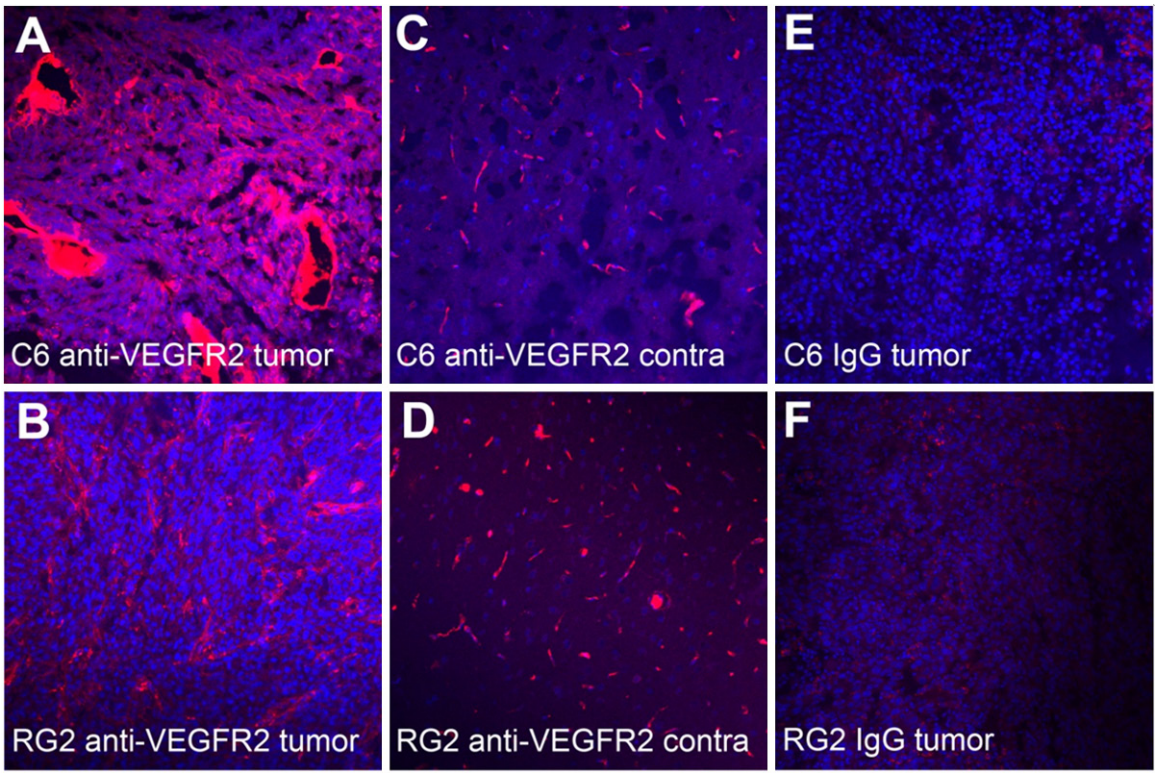

Figure 4. Fluorescence staining of VEGFR2 probe or control-IgG contrast agent in the brain tissue. Glioma tissue post administration of VEGFR2 probe in C6 (A) and RG2 (B) rats. Contralateral brain tissue post administration of VEGFR2 probe in C6 (C) and RG2 (D) rats. Glioma tissue post administration of control-IgG contrast agent in C6 (E) and RG2 (F) rats. Magnification is 60x for Figure 4A-D, and 40x for Figure 4E and 4F. Data was obtained 2 hours following administration of either the anti-VEGFR2 probe or IgG contrast agent.

The contrast difference images (**Figure 2A-ii** for a C6 tumor and **Figure 2B-ii** for a RG2 tumor) were obtained by subtraction of T_1-weighted images before injection and 2 hours post injection. High intensity regions shown on the tumor side of the brain are regions targeted with the VEGFR-2 probe. The signal intensities were calculated from ROIs shown in **Figure 2A-i-D-i**. The increased percentage of signal intensities between the 2-hours post injection images and pre-injection images for the probe or isotype IgG contrast agent are shown in **Figure 3**. For C6 gliomas, most of the probe was concentrated in the tumor periphery (PT) and the peri-necrotic area (PN), compared to the tumor interior (TI) and contralateral tissue (N). However, RG2 gliomas had a relatively even distribution of VEGFR-2 probe levels within the three regions of PT, PN and TI. C6 gliomas had higher VEGFR-2 levels in PT (not significant) and PN (significant; $p<0.05$) regions, but less in TI region (significant; $p<0.01$), compared to RG2 gliomas. The control-IgG resulted in only minimum signal intensity changes in both C6 and RG2 gliomas, and was not found to be significantly different between the two gliomas (data not shown).

Fluorescence staining of VEGFR-2 probes in the brain tissues

Two hours after post administration of the molecular targeting agents, the brain was stained with fluorescence-labeled streptavidin, which binds to the biotin group of the targeting agents. As shown in **Figure 3**, in the tumor periphery region, C6 has more VEGFR2 probe levels concentrated on dilated, large size blood vessels, compared to the RG2 tumor (**Figure 4A-i**, **4B-i**). The contralateral brain has much less probe staining (**Figure 4A-ii**, **4B-ii**), compared to tumor tissues. Both C6 and RG2 gliomas injected with control-IgG contrast agent showed very little staining in the tissue (**Figure 4A-iii**, **4B-iii**). The Mean Fluorescence Intensity (MFI) from excised tumor and contralateral brain tissues, administered either the anti-VEG-

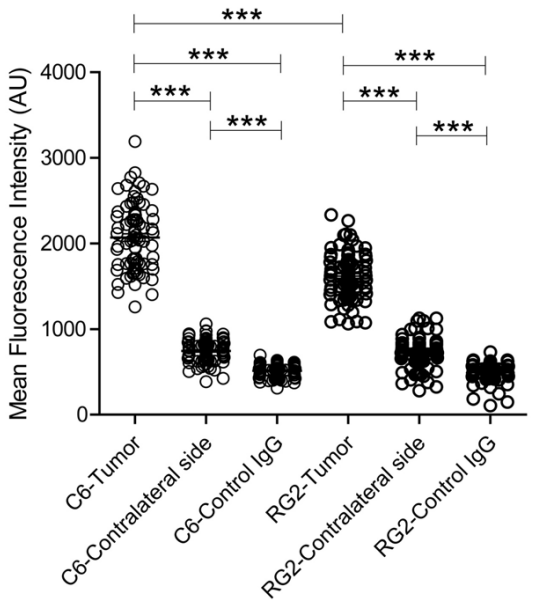

Figure 5. Mean fluorescence intensity (MFI) targeted and non-specific contrast agents evaluated from fluorescence images taken from *ex vivo* tumor periphery and contralateral brain in VEGFR2-probe injected rats, and tumor periphery in control-IgG contrast agent injected rats, respectively. ***p<0.0001 indicates significance between the groups, by using ANOVA with a Tukey's multiple comparison test.

FR2 probe or the non-specific IgG contrast agent, were evaluated (**Figure 5**) and both C6 and RG2 gliomas were found to have significantly higher MFI associated with anti-VEGFR2 probe levels, compared to the contralateral side. It is interesting to note that the MFI in the contralateral sides were higher than those from tumor tissues in animals administered the non-specific control-IgG contrast agent. **Figure 5** also shows that the MFI of C6 tumor (periphery) with a median MFI of 2050, is significantly higher than for the RG2 tumor (periphery), with a median MFI of 1617.

Immunohistochemistry and western blot detection of VEGFR-2

Figure 6A-D depicts the immunohistochemistry (IHC) staining and IHC scoring for levels of VEGFR-2 in C6 and RG2 tumors and their respective contralateral brain tissues. Western blot levels of VEGFR-2 levels in C6 and RG2 glioma tissues seem to indicate a slight increase in C6 gliomas compared to RG2 gliomas (**Figure 6E**). Tumor levels of VEGFR-2, measured as mean fluorescence intensity, in both the C6 and RG2 models were significantly higher when compared to contralateral brain tissues ($p<0.001$ for C6 gliomas, and $p<0.001$ for RG2 tumors) (**Figure 6F**). Levels of VEGFR-2 in C6 gliomas were significantly higher than RG2 tumors ($p<0.001$) (**Figure 6F**).

Immunohistochemistry detection of HIF-1α

Figure 7 depicts the immunohistochemistry (IHC) staining and IHC scoring for levels of HIF-1α in C6 and RG2 tumors and their respective contralateral brain tissues. There was no significant difference in HIF-1α levels in the contralateral brain of C6 and RG2 glioma-bearing tissues (**Figure 7I**). Tumor levels of HIF-1α in both the C6 and RG2 models were significantly higher when compared to contralateral brain tissues ($p<0.01$ for C6 gliomas, and $p<0.001$ for RG2 tumors) (**Figure 7I**). Levels of HIF-1α in RG2 gliomas were significantly higher than C6 tumors ($p<0.01$) (**Figure 7I**). 3D immunofloresecence images from C6 and RG2 glioma sections staining for the endothelial marker laminin indicate large endothelial cells in C6 tumors, compared to more diffuse and increased vasculature in RG2 tumors (**Figure 7G** and **7H**).

Discussion

In this study, VEGFR-2 levels detected by an anti-VEGFR-2 probe associated with glioma type were compared between rat RG2 and C6 glioma models. Although the anti-VEGFR-2 probe may not reflect the absolute concentration of VEGFR-2 in tumor tissue, the method does provide information on a relative and dynamic distribution of VEGFR-2 protein levels *in vivo*. The effectiveness of VEGFR-2 molecular targeting with specific contrast agents were confirmed with fluorescent staining of tumor and normal brain tissues. It was established in our study that VEGFR-2 levels and its distribution were detected in different glioma regions using an anti-VEGFR-2 probe and targeted mMRI. The patterns of VEGFR-2 levels were apparently different between RG2 and C6 gliomas. The C6 tumors showed a more heterogeneous pattern with more VEGFR-2 in the tumor periphery, but less in the tumor interior, compared to RG2 gliomas. This indicates that C6 gliomas have more active angiogenesis occurring in the relatively larger vessels within the tumor periphery, whereas RG2 gliomas have

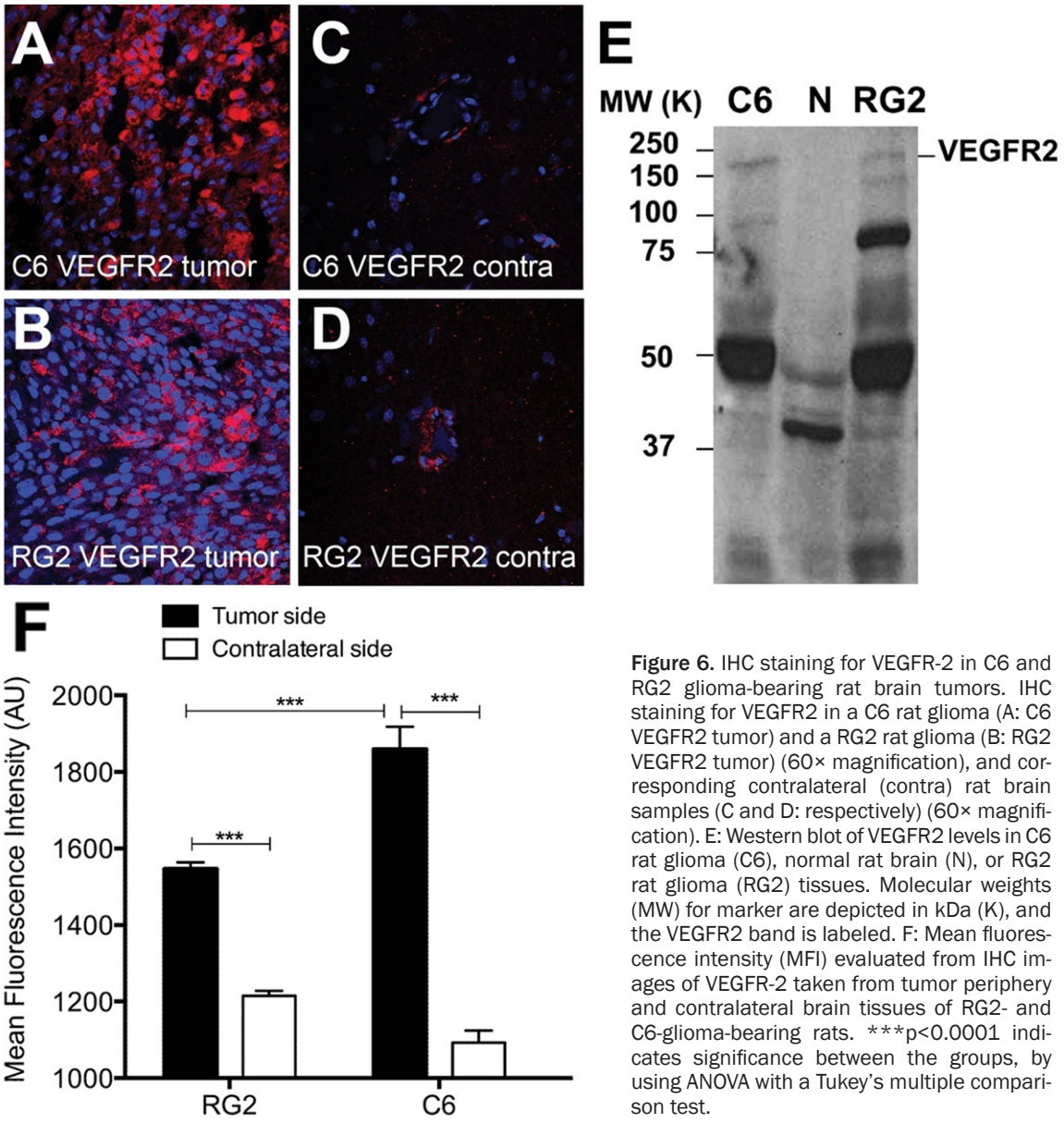

Figure 6. IHC staining for VEGFR-2 in C6 and RG2 glioma-bearing rat brain tumors. IHC staining for VEGFR2 in a C6 rat glioma (A: C6 VEGFR2 tumor) and a RG2 rat glioma (B: RG2 VEGFR2 tumor) (60× magnification), and corresponding contralateral (contra) rat brain samples (C and D: respectively) (60× magnification). E: Western blot of VEGFR2 levels in C6 rat glioma (C6), normal rat brain (N), or RG2 rat glioma (RG2) tissues. Molecular weights (MW) for marker are depicted in kDa (K), and the VEGFR2 band is labeled. F: Mean fluorescence intensity (MFI) evaluated from IHC images of VEGFR-2 taken from tumor periphery and contralateral brain tissues of RG2- and C6-glioma-bearing rats. ***p<0.0001 indicates significance between the groups, by using ANOVA with a Tukey's multiple comparison test.

increased angiogenesis in the capillaries within the tumor interior.

Tumor vasculature has been demonstrated to be abnormal, including discontinuous basement membranes, spatial heterogeneity, arteriovenous shunts, acutely and transiently collapsing vessels and poor differentiation, and a lack of smooth muscle cell lining, resulting in the development of a leaky blood-tumor barrier [21]. During the processes of angiogenesis induced by different glioma cell lines, C6 and RG2 vasculature (including microvessel density, permeability to USPIO) evolves differently, as showed by Valable*et al*. or Beaumount *et al*. [10, 22]. From the Valable study, MRI evaluation of blood volume fraction (BVf) and vessel size index (VSI) was used to assess that the evolution of tumor microvasculature in two rat models of glioma (C6 and RG2) differs significantly between the two glioma models, where BVf was found to be higher in RG2 gliomas and in contrast VSI was assessed to be higher in C6 gliomas [10]. The BVf was also found to be in good agreement with the expression of angiogenic factors (vascular endothelial growth factor, angiopoietin-2) and with activities of matrix metalloproteinases also assessed [10]. Likewise, Beaumont and co-workers found that the C6 and RG2 gliomas presented different blood

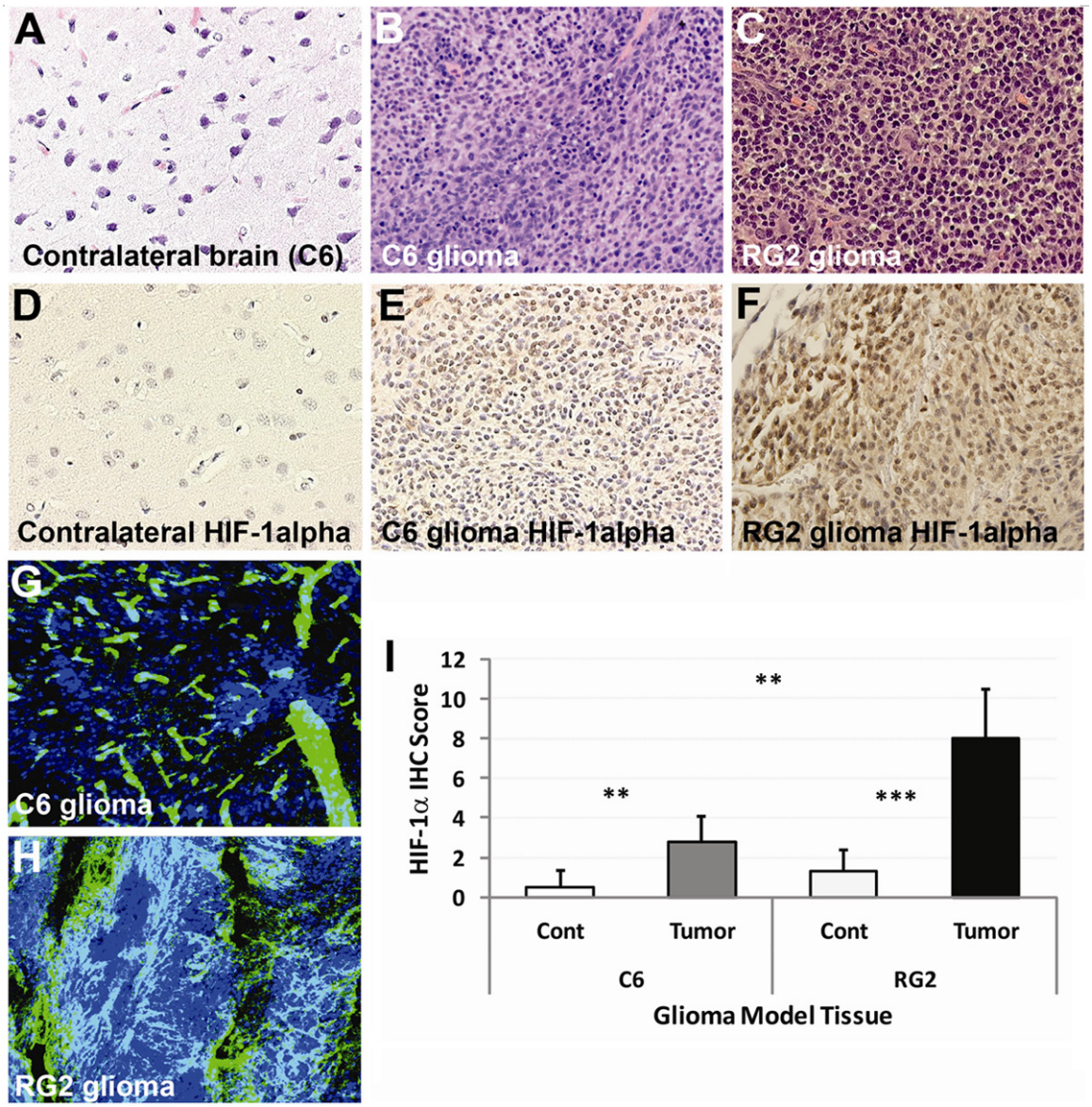

Figure 7. IHC staining for HIF-1α in C6 and RG2 glioma-bearing rat brain tumors. A: Contralateral rat brain tissue H&E histological slide (40× magnification). C6 (B) and RG2 (C) rat glioma H&E histological slides (20× magnification). IHC staining for HIF-1α in a contralateral rat brain sample (D) (40× magnification), C6 rat glioma (E) (20× magnification), and RG2 rat glioma (F) (20× magnification). Maximum intensity projection (MIP) (orthogonal) of confocal optical sections (100-μm thick cryosections) immunostained for laminin (green) and cell nuclei (blue) in C6 (G) and RG2 (H) rat gliomas. I: Histogram of IHC scoring for HIF-1α levels in contralateral and tumor tissues from C6 and RG2 glioma-bearing rats. Data is represented as mean±S.D. **P<0.01, and ***P<0.001, indicates a significant increase in HIF-1α levels in tumor regions, compared to contralateral tissue, in C6 and RG2 glioma-bearing rats, respectively. **P<0.01 (top) indicates a significant increase in HIF-1α levels in RG2 gliomas compared to C6 tumors.

volume fractions and VSI in agreement with the Valable study [22].

Our previous work showed that the RG2 glioma is a relatively more aggressive model with more diffuse margins at the interface to adjacent brain tissue, whereas the C6 gliomas are less infiltrative with a distinct peritumoral region [23]. Both a MRI perfusion study and immunohistochemical detection of the endothelial marker laminin, suggested a higher amount of microvasculature in RG2 gliomas compared to C6 tumors [17], which would correspond with BVf in the Valable or Beaumont studies. This is

also consistent with the signal intensity changes in our current mMRI results. We found that MRI signal enhancement of the VEGFR-2 probe in the RG2 tumor interior is more than twice that for the C6 tumor interior, suggesting more VEGFR-2 from microvessles inside the RG2 tumor. However, compared to C6 gliomas, RG2 gliomas have a relatively more homogeneous pattern for VEGFR-2 levels in the tumor overall (**Figures 2** and **3**). In the C6 glioma, distinctively higher levels of VEGFR-2 were found in peri-tumor and peri-necrotic regions compared to tumor interior regions [14].

In a previous study, we have demonstrated that the target for the specific anti-VEGFR-2 probe, was mainly VEGFR-2 located on endothelial cells, due to co-localization of the anti-VEGFR-2 probe with endogenous VEGFR-2 levels and laminin, an endothelial cell marker [14]. Therefore it was previously established that this probe can be considered as a reliable marker for the evaluation of glioma-induced angiogenesis [14]. Previous assessment of the anti-VEGFR2 probe also indicated that sustained decreases in T_1 relaxation were maintained for at least 24 hours [14]. The Gd-DTPA-albumin construct has been well characterized previously as a vascular contrast agent in various tumor models [24]. In this current MRI study, we found that the C6 tumor periphery (including peri-necrotic region) had almost twice the probe concentrationcompared to the RG2 tumor periphery. This is also confirmed by fluorescence staining of the probe biotin group,indicating that the C6 tumor periphery MFI of the probe exceeds that detected in RG2 tumors by 21% (**Figures 3** and **4**). Fluorescence imaging of the probe also showed a difference in blood vessel morphology between the two models. The tumor blood vessels which were targeted by the MRI probe, that is, the blood vessels undergoing active angiogenesis, were found to be more dilated with increased diameters and thicknesses of the vessel walls in C6 gliomas. These results are supported by the increased VSI in C6 gliomas detected by Valable *et al*., compared to RG2 tumors [10]. This phenomenon may possibly suggest an increased abnormality and disorganization in tumor vasculature for the C6 gliomas, especially in large-diameter periphery main vessel branches, which may cause a reduction in effective blood flow, and thus eventually an increase in tumor-necrosis. This agrees with previous findings where C6 gliomas tend to form large areas of necrosis [17, 25, 26]. We can also speculate that the enhancement of VEGFR2 expression in the C6 tumor periphery increased vascular dysfunction, thus slowingdown tumor growth, which is consistent with the relatively slow growth rate and less infiltrative and aggressive characteristics of C6 tumors, compared to RG2 gliomas.

In order to establish if VEGFR-2 levels differed in RG2 and C6 gliomas, we performed IHC on glioma-bearing rats not administered the anti-VEGFR-2 probe. IHC results for VEGFR-2 indicated that C6 gliomas had significantly higher levels (**p<0.001) compared to RG2 gliomas (**Figure 6E**), which correlated with anti-VEGFR-2 probe levels in **Figure 5**. Therefore, these results confirm that the anti-VEGFR-2 probe is primarily targeting VEGFR-2 in both glioma models.

We also wanted to assess another marker, HIF-1α, for tumor malignancy to verify that the RG2 tumor was a more aggressive tumor. IHC results for HIF-1α indicated that RG2 gliomas had significantly higher levels (**p<0.01) compared to C6 gliomas (**Figure 7**). HIF-1α is commonly used as a marker for tumor malignancy as it is an indicator of poor prognosis in many tumors [27], and has been strongly associated with angiogenesis by stimulating the expression of VEGF via the upregulation of CXCR4 [28]. The immunofluorescence data for laminin (**Figure 7G** and **7H**), an endothelial cell marker, which indicated larger blood vessels in C6 glioma tissue compared to more abundant, smaller and diffuse blood vessels in RG2 tumors, seems to correlate with HIF-1α results. Although VEGR-2 levels in the different glioma models do not seem to correlate with HIF-1α or laminin, as VEGFR-2 levels seem to be higher in the C6 glioma tumors compared to RG2 tumors.

We have also previously shown that permeability for the two tumor types is not substantially different, as detected from dynamic contrast-enhanced (DCE) MRI with the contrast agent Gd-DTPA [17]. In a similar finding by Beaumont *et al*., C6 and RG2 gliomas were also found to be equally permeable to Gd-DOTA [22]. These findings indicate that there is no preferential uptake of the VEGFR-2 probe in either of the two glioma models based on permeability.

The utilization of molecular targeting MRI is one of the most promising imaging modalities for imaging and characterizing *in vivo* angiogenesis [29, 30]. With the use of molecular targeting for VEGFR-2 using an anti-VEGFR-2 probe and MRI, followed by validation that the anti-VEGFR-2 probe was able to detect various VEGFR-2 levels in different glioma models, our studies provide another method for imaging angiogenesis. Other than MRI, VEGF/VEGFR molecular targeting with other imaging modalities, including ultrasound, optical imaging, SPECT and PET has also been done [31, 32]. We detected VEGFR-2 levels with an anti-VEGFR-2 probe with a relatively high image resolution, and good specificity as demonstrated by the low MR signal enhancement in gliomas administrated with control-IgG contrast agent (**Figures 4** and **5**). Another group that used MRI along with a low molecular weight polylysine-$(Gd\text{-}DOTA)_8$-dendron with a peptoid dimer for targeting VEGFR2 found that nude mice with MDA-MB-231 xenografts had significantly increased MRI signal intensities 4 hours following i.v. injection of the VEGFR2 probe [33]. Molecular imaging is also becoming more popular as a method to assess antiangiogenic drug development [34, 35].

Our study was found to differentiate the *in vivo* angiogenic profiles between two different glioma models using an anti-VEGFR-2 probe in conjunction with mMRI. This approach, based on altered VEGFR-2 level detection, could be used as a method for monitoring *in vivo* responses to anti-glioma treatment as well as therapeutic agent dose optimization in pre-clinical models for gliomas and other cancers.

Acknowledgements

Funding was provided by the National Institutes of Health (R03 CA133936-02) and the Oklahoma Center for the Advancement of Science and Technology (AR092049).

Disclosure of conflict of interest

The authors declare that they have no conflict of interest.

Address correspondence to: Rheal A Towner, Advanced Magnetic Resonance Center, Oklahoma Medical Research Foundation, Oklahoma City, OK 73104 USA. Phone: 1-405-271-7383; E-mail: RhealTowner@omrf.org

References

[1] CBTRUS Statistical Report: Primary Brain and Central Nervous System Tumors Diagnosed in the United States in 2004-2007. Central Brain Tumor Registry of the United States (CBTRUS) 2011.

[2] Plate KH, Risau W. Angiogenesis in malignant gliomas. Glia 1995; 15: 339-347.

[3] Folkman J. New perspectives in clinical oncology from angiogenesis research. Eur J Cancer 1996; 32A: 2534-2539.

[4] Vidal S, Kovacs K, Lloyd RV, Meyer FB, Scheithauer BW. Angiogenesis in patients with craniopharyngiomas: correlation with treatment and outcome. Cancer 2002; 94: 738-745.

[5] Ferrara N. Vascular endothelial growth factor: basic science and clinical progress. Endocr Rev 2004; 25: 581-611.

[6] Motzer RJ, Michaelson MD, Redman BG, Hudes GR, Wilding G, Figlin RA, Ginsberg MS, Kim ST, Baum CM, DePrimo SE, Li JZ, Bello CL, Theuer CP, George DJ, Rini BI. Activity of SU11248, a multitargeted inhibitor of vascular endothelial growth factor receptor and platelet-derived growth factor receptor, in patients with metastatic renal cell carcinoma. J Clin Oncol 2006; 24: 16-24.

[7] Lindner V, Reidy MA. Expression of VEGF receptors in arteries after endothelial injury and lack of increased endothelial regrowth in response to VEGF. Arterioscler Thromb Vasc Biol 1996; 16: 1399-1405.

[8] Barth RF. Rat brain tumor models in experimental neuro-oncology: the 9L, C6, T9, F98, RG2 (D74), RT-2 and CNS-1 gliomas. J Neurooncol 1998; 36: 91-102.

[9] Barth RF, Kaur B. Rat brain tumor models in experimental neuro-oncology: the C6, 9L, T9, RG2, F98, BT4C, RT-2 and CNS-1 gliomas. J Neurooncol 2009; 94: 299-312.

[10] Valable S, Lemasson B, Farion R, Beaumont M, Segebarth C, Remy C, Barbier EL. Assessment of blood volume, vessel size, and the expression of angiogenic factors in two rat glioma models: a longitudinal *in vivo* and *ex vivo* study. NMR Biomed 2008; 21: 1043-1056.

[11] Winter PM, Caruthers SD, Kassner A, Harris TD, Chinen LK, Allen JS, Lacy EK, Zhang H, Robertson JD, Wickline SA, Lanza GM. Molecular imaging of angiogenesis in nascent Vx-2 rabbit tumors using a novel alpha(nu)beta3-targeted nanoparticle and 1.5 tesla magnetic resonance imaging. Cancer Res 2003; 63: 5838-5843.

[12] Kang HW, Torres D, Wald L, Weissleder R, Bogdanov AA Jr. Targeted imaging of human endo-

thelial-specific marker in a model of adoptive cell transfer. Lab Invest 2006; 86: 599-609.
[13] Persigehl T, Bieker R, Matuszewski L, Wall A, Kessler T, Kooijman H, Meier N, Ebert W, Berdel WE, Heindel W, Mesters RM, Bremer C. Antiangiogenic tumor treatment: early noninvasive monitoring with USPIO-enhanced MR imaging in mice. Radiology 2007; 244: 449-456.
[14] He T, Smith N, Saunders D, Doblas S, Watanabe Y, Hoyle J, Silasi-Mansat R, Lupu F, Lerner M, Brackett DJ, Towner RA. Molecular MRI assessment of vascular endothelial growth factor receptor-2 in rat C6 gliomas. J Cell Mol Med 2011; 15: 837-849.
[15] Doblas S, Saunders D, Kshirsagar P, Pye Q, Oblander J, Gordon B, Kosanke S, Floyd RA, Towner RA. Phenyl-tert-butylnitrone induces tumor regression and decreases angiogenesis in a C6 rat glioma model. Free Radic Biol Med 2008; 44: 63-72.
[16] Benda P, Lightbody J, Sato G, Levine L, Sweet W. Differentiated rat glial cell strain in tissue culture. Science 1968; 161: 370-371.
[17] Towner RA, Smith N, Doblas S, Garteiser P, Watanabe Y, He T, Saunders D, Herlea O, Silasi-Mansat R, Lupu F. *In vivo* detection of inducible nitric oxide synthase in rodent gliomas. Free Radic Biol Med 2010; 48: 691-703.
[18] Dafni H, Landsman L, Schechter B, Kohen F, Neeman M. MRI and fluorescence microscopy of the acute vascular response to VEGF165: vasodilation, hyper-permeability and lymphatic uptake, followed by rapid inactivation of the growth factor. NMR Biomed 2002; 15: 120-131.
[19] Hermanson GT. Bioconjugate Techniques. New York: Academic Press 1996; pp: 176.
[20] Lupu C, Westmuckett AD, Peer G, Ivanciu L, Zhu H, Taylor FB Jr, Lupu F. Tissue factor-dependent coagulation is preferentially up-regulated within arterial branching areas in a baboon model of Escherichia coli sepsis. Am J Pathol 2005; 167: 1161-1172.
[21] Pathak AP, Penet MF, Bhujwalla ZM. MR molecular imaging of tumor vasculature and vascular targets. Adv Genet 2010; 69: 1-30.
[22] Beaumont M, Lemasson B, Farion R, Segebarth C, Remy C, Barbier EL. Characterization of tumor angiogenesis in rat brain using iron-based vessel size index MRI in combination with gadolinium-based dynamic contrast-enhanced MRI. J Cereb Blood Flow Metab 2009; 29: 1714-1726.
[23] Doblas S, He T, Saunders D, Pearson J, Hoyle J, Smith N, Lerner M, Towner RA. Glioma morphology and tumor-induced vascular alterations revealed in seven rodent glioma models by in vivo magnetic resonance imaging and angiography. J Magn Reson Imaging 2010; 32: 267-275.
[24] Bhujwalla ZM, Artemov D, Natarajan K, Ackerstaff E, Solaiyappan M. Vascular differences detected by MRI for metastatic versus nonmetastatic breast and prostate cancer xenografts. Neoplasia 2001; 3: 143-53.
[25] He T, Doblas S, Saunders D, Casteel R, Lerner M, Ritchey JW, Snider T, Floyd RA, Towner RA. Effects of PBN and OKN007 in rodent glioma models assessed by 1H MR spectroscopy. Free Radic Biol Med 2011; 51: 490-502.
[26] Grobben B, De Deyn PP, Slegers H. Rat C6 glioma as experimental model system for the study of glioblastoma growth and invasion. Cell Tissue Res 2002; 310: 257-270.
[27] Du R, Lu KV, Petritsch C, Liu P, Ganas R, Passegué E, Song H, Vandenberg S, Johnson RS, Werb Z, Bergers G. HIF1alpha induces the recruitment of bone marrow-derived vascular modulatory cells to regulate tumor angiogenesis and invasion. Cancer Cell 2008; 13: 206-20.
[28] Zagzag D, Lukyanov Y, Lan L, Ali MA, Esencay M, Mendez O, Yee H, Voura EB, Newcomb EW. Hypoxia-inducible factor 1 and VEGF upregulate CXCR4 in glioblastoma: implications for angiogenesis and glioma cell invasion. Lab Invest 2006; 86: 1221-32.
[29] McDonald DM, Choyke PL. Imaging of angiogenesis: from microscope to clinic. Nat Med 2003; 9: 713-725.
[30] Mulder WJ, Griffioen AW. Imaging of angiogenesis. Angiogenesis 2010; 13: 71-74.
[31] Cai W, Chen X. Multimodality imaging of vascular endothelial growth factor and vascular endothelial growth factor receptor expression. Front Biosci 2007; 12: 4267-4279.
[32] Cai W, Chen X. Multimodality molecular imaging of tumor angiogenesis. J Nucl Med 2008; 49 Suppl 2: 113S-128S.
[33] De León-Rodriguez LM, Lubag A, Udugamasooriya DG, Proneth B, Brekken RA, Sun X, Kodadek T, Sherry AD. MRI detection of VEGFR2 *in vivo* using a low molecular weight peptoid-(Gd)8-dendron for targeting. J Am Chem Soc 2010; 132: 12829-31.
[34] Cai W, Rao J, Gambhir SS, Chen X. How molecular imaging is speeding up antiangiogenic drug development. Mol Cancer Ther 2006; 5: 2624-2633.
[35] Winter PM, Caruthers SD, Allen JS, Cai K, Williams TA, Lanza GM, Wickline SA. Molecular imaging of angiogenic therapy in peripheral vascular disease with alphanubeta3-integrin-targeted nanoparticles. Magn Reson Med 2010; 64: 369-376.